ACS APPLIED MATERIALS & INTERFACES

Research Article

www.acsami.org

Hyaluronic Acid Oligosaccharide Modified Redox-Responsive Mesoporous Silica Nanoparticles for Targeted Drug Delivery

Qinfu Zhao,[†] Hongjian Geng,[†] Ying Wang,[†] Yikun Gao,[‡] Jiahao Huang,[†] Yan Wang,[§] Jinghai Zhang,[‡] and Siling Wang*,[†]

[†]Department of Pharmaceutics, School of Pharmacy, Shenyang Pharmaceutical University, 103 Wenhua Road, Shenyang 110016, People's Republic of China

[‡]School of Medical Devices, Shenyang Pharmaceutical University, 103 Wenhua Road, Shenyang 110016, People's Republic of China

[§]Department of Physical Chemistry, School of Pharmacy, Shenyang Pharmaceutical University, 103 Wenhua Road, Shenyang 110016, People's Republic of China

ABSTRACT: A redox-responsive delivery system based on colloidal mesoporous silica (CMS) has been developed, in which 6-mercaptopurine (6-MP) was conjugated to vehicles by cleavable disulfide bonds. The oligosaccharide of hyaluronic acid (oHA) was modified on the surface of CMS by disulfide bonds as a targeting ligand and was able to increase the stability and biocompatibility of CMS under physiological conditions. In vitro release studies indicated that the cumulative release of 6-MP was less than 3% in the absence of glutathione (GSH), and reached nearly 80% within 2 h in the presence of 3 mM GSH. Confocal microscopy and fluorescence-activated cell sorter (FACS) methods were used to evaluate the cellular uptake performance of fluorescein isothiocyanate (FITC) labeled CMS, with and without oHA modification. The CMS-SS-oHA exhibited a higher cellular uptake performance via CD44 receptor-mediated endocytosis in HCT-116 (CD44 receptor-positive) cells than in NIH-3T3 (CD44 receptor-negative) cells. 6-MP loaded CMS-SS-oHA exhibited greater cytotoxicity against HCT-116 cells than NIH-3T3 cells due to the enhanced cell uptake behavior of CMS-SS-oHA. This study provides a novel strategy to covalently link bioactive drug and targeting ligand to the interiors and exteriors of mesoporous silica to construct a stimulus-responsive targeted drug delivery system.

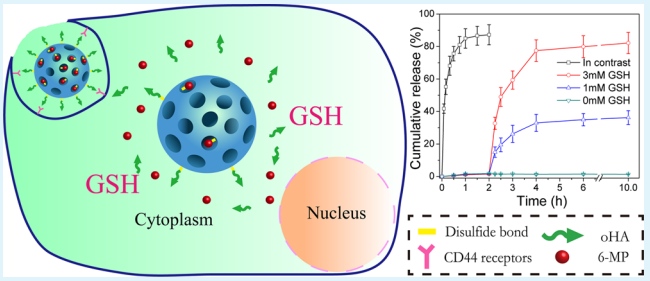

KEYWORDS: *colloidal mesoporous silica, redox-responsive, 6-mercaptopurine, oligosaccharide of hyaluronic acid, CD44 receptors*

1. INTRODUCTION

In recent decades, numerous efforts have been devoted to the development of safe and effective drug delivery systems (DDS) for selective delivery of toxic drugs to tumors.[1,2] Although considerable progress has been made, targeted DDS still have some limitations, mainly involving premature drug release before reaching the target site. An ideal DDS needs to deliver the toxic drug to specific target sites or target cells without drug leakage on the way, then be internalized via a specific interaction with receptors on tumor cells and, finally, rapidly release the drug at the target sites according to environmental stimuli. Hence, active targeting and stimuli-responsive drug release are two important keys to increase the therapeutic efficacy and reduce the side-effects of anticancer drugs.

Recently, stimuli-responsive DDS that release loaded drugs in response to various internal or external stimuli, such as changes in redox potential,[3,4] pH,[3,5,6] enzymes,[7] and temperature, have received widespread attention. Some strategies based on the conjugation of drugs to vehicles by stimuli-responsive bonds have been developed to achieve a "zero premature release".[8] The disulfide bond, a redox-responsive bond, is cleaved under a high concentration of glutathione (GSH), which is a widely studied intracellular signal. The advantage of this covalent bond is its relative stability in extracellular fluids and plasma, and easy rupture in intracellular fluid due to a significant difference in the concentration of GSH between extracellular fluids (2−20 μM) and intracellular fluids (1−10 mM).[9] Furthermore, the cytosolic GSH concentration in tumor cells is at least 3-fold higher than that in normal cells.[10]

Compared with traditional lipid-based nanoparticles or organic polymers,[11] their inorganic counterparts exhibit particular properties such as inertness and chemical stability. Specifically, the prominent characteristics of mesoporous silica nanoparticles (MSNs), such as their high surface area, tunable pore size, ease of surface functionalization, and excellent biocompatibility, make these vehicles ideal candidates for the development of stimuli-responsive DDS.[12,13] In this paper, we

Received: August 28, 2014
Accepted: October 14, 2014
Published: October 14, 2014

Scheme 1. GSH-Responsive Drug Release in the Tumor Cells and Magnified Image of Pore Structure[a]

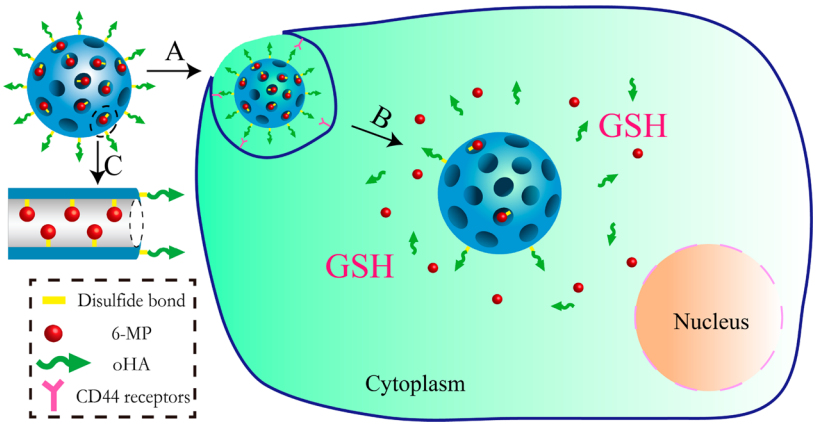

[a](A) Cellular uptake through oHA mediated CD44 interaction, (B) GSH triggered drug release inside the cell, (C) magnified image of pore structure of CMS-SS-MP/oHA.

describe the use of a redox-responsive disulfide bond to connect a mercapto-containing drug to mercapto-functionalized silica. Although only a limited number of drugs contain a mercapto group, some anticancer drugs, such as doxorubicin and cisplatin, can accept a mercapto group by a simple modified grafting process, and then be covalently grafted to silica by disulfide bonds.[14,15]

Hyaluronic acid (HA), also called hyaluronan, is a very large, anionic, biodegradable, linear polysaccharide composed of 1000−25 000 repeated units of glucuronic acid and *N*-acetylglucosamine.[16,17] HA has been widely used for DDS due to a specific interaction with CD44 receptors that are overexpressed on various cancer cells.[17−19] The strategy of HA modified MSNs for the tumor targeting delivery and improved dispersity has been reported previously.[20−22] However, there are some limitations to the use of macromolecular HA as a target or drug carrier, such as its rapid clearance and destruction by the liver due to its relatively low solubility in blood. The main differences in our work are the molecular weight of HA and the chemical bonds which link the targeting ligand to the surface of silica. First, macromolecular HA can be degraded into oligosaccharides (fragments) of HA (oHA) with a Mw <10 000 by hyaluronidase. It is also known that oHA can compete for binding of endogenous macromolecular HA to its receptors, leading to the replacement of the HA that is already bound to CD44 receptors.[23,24] In addition, oHA has some attractive characteristics, including a longer blood circulation time and slow removal from liver, compared with native HA.[25] Second, oHA was modified on the surface of silica by cleavable disulfide bonds rather than the amido bond. The main function of targeting ligand is to increase the cellular uptake of DDS. However, the surface targeting group might retard the release of drugs after the DDS is uptaked by tumor cells,[26] especially for a high molecular weight targeting ligand. Therefore, in the present work, the oHA was modified on the surface of silica by means of a cleavable disulfide bond. Until now, there have been no published reports of using oHA as a target moiety to increase the cellular uptake of stimuli-responsive DDS.

In the present work, stable thiol-functionalized colloidal mesoporous silica (CMS-SH) nanoparticls with a uniform particle size of 80 nm were synthesized as stimuli-responsive targeted drug nanocarriers. The compound, 6-mercaptopurine (6-MP), an antimetabolite with a mercapto group, was chosen as a model drug to be loaded into the pores of silica by cleavable disulfide bonds. Then, oHA was grafted to the outer layer of CMS by disulfide bonds in order to selectively target tumors cells and increase the biocompatibility and dispersibility of silica. The schematic illustration of cellular uptake and GSH triggered drug release is shown in Scheme 1. The specificity of oHA for CD44 receptors was investigated in HCT-116 (receptor-positive) and NIH-3T3 (receptor-negative) cell lines. Moreover, 6-MP loaded CMS-SS-MP/oHA had a more potent effect in HCT-116 cells than free 6-MP or CMS-SS-MP/oHA in NIH-3T3 cells. The delivery system has tremendous potential for tumor targeted delivery and intracellular redox-responsive drug release.

2. EXPERIMENTAL SECTION

2.1. Materials. Fluorescein isothiocyanate (FITC), 3-mercaptopropyltrimethoxysilane (MPTMS, 95%), 2,2′-dipyridyl disulfide, 6-mercaptopurine (6-MP), cysteamine hydrochloride, *N*-(3-(dimethylamino)propyl)-*N*-ethylcarbodiimide hydrochloride (EDC), *N*-hydroxysuccinimide (NHS), and glutathione (GSH) were obtained from Sigma-Aldrich Chemical (St. Louis, MO, USA). Tetraethoxysilane (TEOS), triethanolamine (TEA), and cetyltrimethylammonium chloride (CTAC) were obtained from Tianjin Bodi Chemical Holding Co., Ltd. (Tianjin, China). 3-(4,5-Dimethylthiazol-2-yl)-2,5-diphenyl tetrazolium bromide (MTT) and bovine serum albumin (BSA) were supplied by Amresco (USA). The oHA was a product of Shandong Freda Biochem Co. Ltd. (China). Cell culture Dulbecco's modified Eagle's medium (DMEM), penicillin-streptomycin, and fetal bovine serum (FBS) were obtained from GIBCO, Invitrogen Co. (Carlsbad, CA, USA). Fluorescent Hoechst 33258, rhodamine-phalloidin were bought from Molecular Probes Inc. (Eugene, OR, USA). All other chemicals were of analytical grade as required and used without further purification.

2.2. Preparation of CMS-SH. The CMS-SH nanoparticles were prepared according to the published literature.[27] In brief, 64 mL of distilled water, 10.5 mL of ethanol, and 10.4 mL of 25 wt % CTAC were violently stirred for 10 min at room temperature. 4.125 mL of TEA was subsequently added and the solution was stirred for 15 min. Then 40 mL of the solution was heated to 60 °C, followed by the dropwise addition of a mixture of 2.9 mL of TEOS and 0.5 mL of MPTMS under stirring. After the solution was stirred for 2 h, the obtained suspension was homogenized by an ATS AH100D homogenizer at 800 bar for five cycles to reduce the aggregation of nanoparticles (ATS Engineer Inc., Shanghai, China). Finally, the resulting product was centrifuged, washed with distilled water and ethanol for three times, and dried under vacuum for 12 h.

2.3. Synthesis of S-(2-Aminoethylthio)-2-thiopyridine Hydrochloride (Py-SS-NH_2). The synthesis of the compound was according to a literature report.[28] Typically, 4.4 g of thiopyridyldisulfide was dissolved in 20 mL of methanol, and 0.8 mL acetic acid was added. 10 mL of methanol solution containing 2-aminoethylthiolhydrochloride (1.14 g) was added dropwise into the mixture over a period of 15 min. The reaction mixture was stirred for an additional 48 h, and then evaporated under high vacuum to leave a yellow oil. The product was washed with 50 mL of diethyl ether and then dissolved in 10 mL of methanol. The product was precipitated by the addition of diethyl ether (200 mL), chilled at −20 °C for 24 h, and then collected by vacuum filtration. The product was reprecipitated in methanol (10 mL) in order to obtain a pure compound.

2.4. Synthesis of CMS-SS-NH_2 Nanoparticles. The introduction of disulfide bonds and terminal ammonium was realized by suspending 500 mg of CMS-SH without the template extraction in ethanol (25 mL), and then followed by the addition of 200 mg of Py-SS-NH_2. The mixture was stirred at room temperature for 36 h. Then the product was collected by centrifugation and washed with ethanol. To remove the template CTAC, the product was refluxed for two times in a solution of 160 mL of methanol and 9 mL of HCl (37%) at 80 °C for 12 h, and then the surfactant-removed samples were centrifuged, washed with ethanol and distilled water, and dried under vacuum for 12 h.

2.5. Drug Loading for CMS-SS-MP/oHA. For desalting, 500 mg of oligosaccharides of sodium hyaluronate (<10 K) was dissolved into a dialysis bag (cutoff Mw = 1000 g mol^{-1}), and the dialysis bag was put into the 5 L of deionized water with magnetic stirring at room temperature for 12 h. During this desalting process, the deionized water was replaced for five times to ensure complete desalting. The resulting oHA was lyophilized and kept in 4 °C.

The drug loading process was as follows. First, 100 mg of 6-MP was dissolved in 7 mL of dimethyl sulfoxide (DMSO), and then 3 mL of iodine DMSO solution (30 mg/mL) was added dropwise to oxidize 6-MP. The mixed solution was stirred at room temperature for 24 h. Then 200 mg of CMS-SS-NH_2 was added to the solution under a N_2 atmosphere to minimize air oxidation, and further stirred for 24 h to allow the disulfide bonds exchange reaction to take place. The resulting product was centrifuged and washed with DMSO and ethanol for two times. The oHA was grafted on the surface of silica to target CD44 receptors overexpressing tumor cells and improve the dispersibility of the nanoparticles. Briefly, 60 mg of oHA was hydrated in distilled water at room temperature and then activated by EDC (3 mg mL^{-1}) and NHS (2 mg mL^{-1}) for 1 h. Then, ca. 200 mg of 6-MP loaded CMS-SS-NH_2 samples was added to the solution under a N_2 atmosphere, followed by stirring for another 24 h. The resulting nanoparticles were centrifuged, washed with water and ethanol, and dried under vacuum for 12 h. The loaded sample after the grafting of oHA was referred to as CMS-SS-MP/oHA.

To further evaluate the redox-responsive release property, the CMS-SH after template extraction was used as the carrier to load 6-MP by an adsorption method (noncovalent interaction). The 6-MP loaded CMS-SH sample was named CMS/MP. The load efficiency of 6-MP was measured by dispersing ca. 15 mg of the 6-MP loaded samples into 100 mL of pH 1.2 hydrochloric acid. And sufficient GSH was added to ensure the complete breakage of the disulfide bonds. The concentration of 6-MP was measured on a UV−vis spectrophotometer (UV-2000, Unico, USA) at 320 nm.

The oHA modified CMS blank carrier (CMS-SS-oHA) was prepared to evaluate the biocompatibility and cellular uptake. The preparation method was as follows. 200 mg of CMS-SS-NH_2 was added into the oHA activated solution, and the resulting solution was further stirred for 24 h. The resulting nanoparticles were centrifuged, washed, and dried under vacuum for 12 h.

2.6. Reduction-Responsive Drug Release. The reduction-responsive release was carried out in a pH 7.4 phosphate buffer solution (PBS) (KC-8D, Tianjin Guoming Medical Equipment Co. Ltd., China). Release studies were measured at 37 °C with a paddle speed of 75 rpm. 15 mg of 6-MP loaded samples was dispersed in 100 mL of PBS medium at zero time. 4 mL of the release medium was withdrawn at predetermined intervals and passed through a 0.22 μm membrane filter. Then, an equal volume of fresh released medium was added to keep the volume constant. The amount of released 6-MP was determined with UV detection at 320 nm.

2.7. Characterization. Scanning electron microscopy (SEM) images were obtained on a SUPRA 35 (ZEISS, Oberkochen, Germany). Transmission electron microscopy (TEM) images were obtained on a Tecnai G2 F30 (FEI, Eindhoven, The Netherlands) operated at a voltage of 200 kV. Nitrogen adsorption−desorption analysis was measured on an adsorption analyzer (V-Sorb 2800P, Beijing, China). The surface areas and pore size distribution were calculated according to Brunauer−Emmett−Teller (BET) and Barrett−Joyner−Halenda (BJH) methods. Particle sizes and ζ-potentials were measured on a Nano-zs90 Nanosizer (Malvern Instruments Ltd., Malvern, UK), and the samples were dispersed in deionized water. Thermogravimetric analysis (TGA) was carried out on a TGA-50 instrument (Shimadzu, Kyoto, Japan) with a heating rate of 5 °C/min under nitrogen flow. Raman spectra were recorded with a LabRam HR800 Raman spectrometer (Jobin Yvon, Paris, France) using a laser excitation wavelength of 532 nm at room temperature. Fourier transform infrared (FT-IR) spectra was measured on a FT-IR spectrometer (Bruker IFS 55, Fällanden, Switzerland) using the KBr pellet technique. The colloidal stability of CMS-SS-oHA in distilled water and pH 7.4 PBS was investigated by turbidity measurements. The measuring wavelength (λ) was chosen as 500 nm. The concentration of 6-MP was measured by UV−vis spectrophotometry (UV-2000, Unico, Dayton, NJ, USA) at 320 nm.

2.8. BSA Adsorption Measurements. The BSA adsorption measurements were studied according to the published method.[29,30] 60 mg of BSA was dissolved in 100 mL of distilled water. 10 mg of CMS-SH and CMS-SS-oHA were respectively dispersed into 5 mL of PBS solution, and then 5 mL of BSA solution was added. The mixture was placed in a shaker at 37 °C with a shaking rate of 135 rpm. After 4 h, the mixure was centrifuged, and then the upper clear solution was collected. Finally, the BSA clear solution was stained with Coomassie brilliant blue solution and measured on a UV−vis measurement at 595 nm. The adsorbed BSA was calculated using the following equation:

$$q = (C_i - C_f)V/m$$

where C_i and C_f are the initial and final BSA concentrations in the solution before and after BSA adsorption, respectively; V is the total solution volume; m is the weight of nanoparticles added into the solution.

2.9. Hemolysis Assay. The rabbit red blood cells (RBCs) were collected at 1000 r/min for 10 min and washed with saline for three times. The RBCs were diluted with saline to a concentration of 2% (v:v). Then 2 mL of the saline solutions of CMS-SH and CMS-SS-oHA were added into the equal volume of RBCs solutions, respectively, and the final concentrations of the nanoparticles were 20, 50, 100, 200, 500, 1000, and 1500 μg/mL. The mixed solutions were kept static for 4 h. Subsequently, the mixtures were centrifuged and the upper clear solutions were taken out and measured at 541 nm on a UV−vis spectrophotometer. The hemolysis of RBCs in distilled water and saline was used as the positive and negative control, respectively. Hemolysis percentages (%) = (absorbances of the sample − absorbances of negative control)/(absorbances of the positive control − absorbances of negative control) × 100.

2.10. FITC Modification of CMS-SH and CMS-SS-oHA. To graft FITC onto silica matrixes, we first covalently linked 2 mg of FITC to 20 μL of APTMS in 2 mL of ethanol in the dark for 12 h. Then, 200 mg of CMS-SH or CMS-SS-NH_2 was dispersed in 20 mL of ethanol and the solution was mixed with 2 mL of FITC/APTMS ethanol solution (1 mg mL^{-1}). After the solution was stirred under dark conditions for 24 h, the nanoparticles were centrifuged and washed with ethanol until the supernatants were colorless and then the oHA was grafted on to the FITC labeled CMS-SS-NH_2 by an amidation reaction.

2.11. Cell Culture and in Vitro Targeting Test. HCT-116 and NIH-3T3 cells were cultured in DMEM supplemented with 10% FBS, 1% penicillin, 1% L-glutamine, and 1% streptomycin in 5% CO_2 at 37

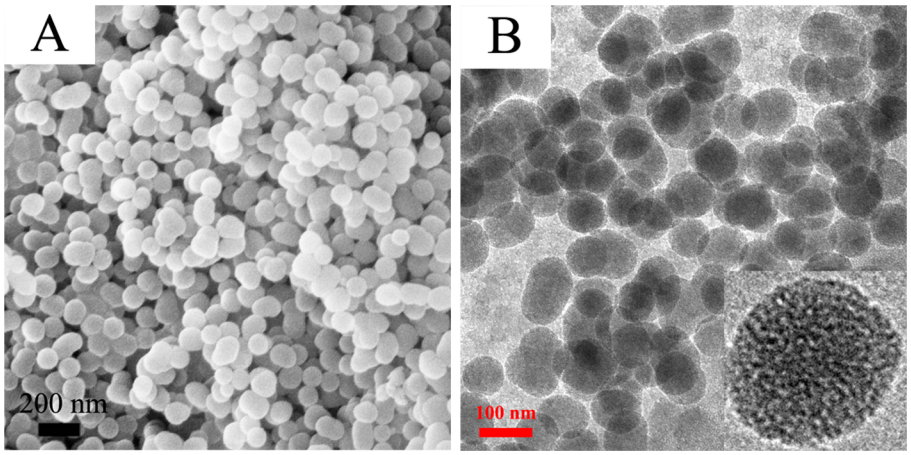

Figure 1. SEM (A) and TEM (B) of CMS-SH nanoparticles.

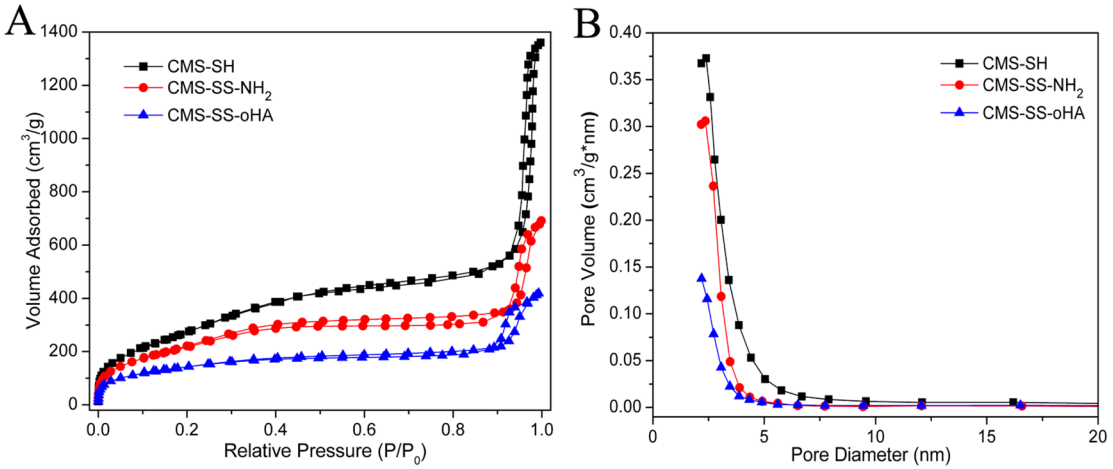

Figure 2. N_2 adsorption/desorption isotherms (A) and pore size distributions (B) of CMS-SH, CMS-SS-NH_2, and CMS-SS-oHA.

°C. The medium was routinely changed every 2 days and the cells were separated by trypsinisation before reaching confluency. The in vitro targeting test was carried out by confocal laser scanning microscopy (CLSM) using HCT-116 and NIH-3T3 cells. HCT-116 and NIH-3T3 cells were seeded in 24-well culture plates at a density of 5×10^4 cells per well and allowed to adhere overnight. After the plates were washed three times with PBS, the cells were incubated with 50 μg mL^{-1} FITC labeled CMS or CMS-SS-oHA in 0.5 mL of serum-free DMEM medium for 2 h at 37 °C. Then, at preselected time intervals, culture medium was removed and the cells were washed three times with cold PBS and fixed with 4% formaldehyde for 20 min at 37 °C. After the cells were stained with Hoechst 33258 for nuclei, the slides were observed using a Leica DM-6000 CS microscope (Leica Instruments Inc., Wetzlar, Germany). Quantitative determination of the cellular uptake was carried out on a fluorescence-activated cell sorter (FACS). HCT-116 and NIH-3T3 cells were seeded in a 6-well plate (5×10^5) and cultured as described above. After incubation with 100 μg mL^{-1} FITC labeled CMS or CMS-SS-oHA for 2 h, the cells were washed three times with cold PBS, trypsinized, and resuspended in PBS. The cells containing FITC-labeled nanoparticles were measured using a flow cytometer (FACSCalibur, Becton Dickinson, Franklin Lakes, NJ, USA). In competitive inhibition experiments, 5 mg mL^{-1} oHA was applied and incubated with HCT-116 cells for 2 h before the nanoparticles were added.

2.12. Cytotoxicity of CMS-SS-MP/oHA and Blank CMS-SS-oHA. An MTT (3-(4,5-dimethylthiazol-2-yl)-2,5-diphenyltetrazolium bromide) assay was used to investigate the cytotoxic effects of 6-MP, blank CMS-SS-oHA, and 6-MP-loaded CMS-SS-MP/oHA nanoparticles on HCT-116 and NIH-3T3 cells. In brief, HCT-116 cells and NIH-3T3 cells were seeded into 96-well plates at a density of 2×10^4 cells per well. After a 24 h incubation period, the serum-free DMEM medium containing serial concentrations of the 6-MP (0.01, 0.1, 1.0, 5.0, 10.0, and 30.0 μg/mL) formulation was added to displace the old cell culture medium. In addition, a series of concentrations, equivalent to those in 6-MP-loaded nanoparticles, of empty CMS-SS-oHA nanoparticles were added to investigate the cytotoxicity of the blank nanocarriers. After a predetermined incubation time, 50 μL of MTT PBS (2 mg/mL) was added to the culture medium and incubation was carried out for another 4 h to quantify the living cells. Then, the DMEM medium was removed and 150 μL of DMSO was added. Finally, the 96-well plates were measured on an iMark microplate reader (Bio-RAD, Hercules, CA, USA) at 570 nm.

2.13. Statistical Analysis. Statistical analysis was performed by Student's *t*-test using SPSS statistical software with p values <0.05 being considered to show statistically significant differences.

3. RESULTS AND DISCUSSION

3.1. Synthesis and Characterization of Functionalized CMS. CMS-SH was prepared by a co-condensation method, involving the simultaneous condensation of TEOS and MPTMS, to obtain a homogeneous distribution of mercapto groups on the internal and external surface of the CMS carrier. The morphology and pore structure of the CMS-SH nanoparticles were characterized by SEM and TEM, respectively. As shown in Figure 1A, the prepared CMS-SH had a uniform spherical shape with a diameter of ca. 80 nm. The TEM image

(Figure 1B) showed that CMS-SH nanoparticles were spherical in shape with a wormhole arrangement of the mesopores.

To graft oHA onto the surface of the CMS nanoparticles, CMS-SH was reacted with Py-SS-NH_2 to introduce terminal ammonium groups. The adsorption−desorption isotherms and pore size distributions of CMS-SH, CMS-SS-NH_2, and CMS-SS-oHA samples are shown in Figure 2. The BET surface area (S_{BET}), total pore volume (V_t), and average pore diameter (D_p) are summarized in Table 1. It can be seen from Table 1 that there were obvious decreases in S_{BET} and V_t of CMS nanoparticles after different functionalized grafting.

Table 1. N_2 Adsorption−Desorption Parameters of Different Functionalized CMS Nanoparticles

sample	S_{BET} (m^2/g)	V_t (cm^3/g)	D_p (nm)
CMS-SH	1018	1.99	2.3
CMS-SS-NH_2	861	0.93	2.3
CMS-SS-oHA	523	0.52	<2

3.2. Drug Loading and Characterization. The anticancer drug 6-MP with a mercapto group was used as the model drug in the present study. The drug loading involved a combination of 6-MP oxidation and a disulfide bond exchange reaction. First, 6-MP was oxidized to 1,2-di(purin-6-yl) disulfane (MP-SS-MP) by iodine and then MP-SS-MP was reacted with the mercapto groups of CMS by a disulfide bond exchange reaction. oHA was grafted on to the surface of the silica to target CD44 receptors, increase the silica dispersibility and prolong the circulation time after intravenous administration. 6-MP and oHA were both grafted onto the silica via a disulfide bond and so CMS-SH without template extraction was initially reacted with Py-SS-NH_2 to transform the surface mercapto groups into disulfide bonds and terminal ammonium groups. Then, a sample of CMS-SS-NH_2 containing surfactants was refluxed to remove the template and expose the internal mercapto groups. Finally, 6-MP was loaded in the CMS-SS-NH_2 by a disulfide bond exchange reaction, followed by grafting of oHA to the silica surface by an amide reaction.

The successful grafting of the disulfide bonds was confirmed by a Raman spectrometer and FT-IR spectra. As shown in Figure 3A, two υ_{ss} Raman stretch bands at 511 cm^{-1} [type (H, H)] and 527 cm^{-1} [type (H, C)] were observed in the CMS-SS-NH_2 sample. For di-primary-alkyl disulfides, two υ_{ss} stretch bands coming from the two conformers [type (H, H) and type (H, C)] were assigned to the CH_2−S−S−CH_2 segment, which indicated that the disulfide bonds were successfully formed.[31] A comparison of the FT-IR spectra of CMS-SH and CMS-SS-NH_2 is shown in Figure 3B. The presence of the mercapto group on CMS-SH was confirmed by the minor peak around 2560 cm^{-1}. After CMS-SH reacted with Py-SS-NH_2, the appearance of a peak around 1525 cm^{-1} was characteristic of the amino group, while the minor peak of mercapto groups around 2560 cm^{-1} disappeared, indicating the formation of CMS-SS-NH_2. In addition, the successful grafting of oHA by amide bond was validated by ζ-potential measurements and thermogravimetric analysis (TGA). The ζ-potentials of the corresponding samples were measured in deionized water at each step to confirm the successful modification of CMS. As shown in Figure 4A, the ζ-potential of CMS-SH without template extraction was +3.99 mV due to the cationic surfactant CTAC. Then, the ζ-potential increased from +3.99 mV to a highly positive value of +31.3 mV after the formation of CMS-SS-NH_2 due to the amine groups on the silica surface. After the samples were grafted with oHA, the ζ-potential converted to a negative value of −25.5 mV. Generally, nanoparticles with a ζ-potential below −25 mV are believed to be colloidally stable.[32] In addition, the ζ-potential of 6-MP loaded CMS-SS-NH_2 and CMS-SS-MP/oHA were +34.6 mV and −27.9 mV. The ζ-potentials of 6-MP loaded samples were not significantly different from those of the 6-MP free samples, which might be attributed to the fact that the 6-MP were loaded in the internal mesopores of CMS. The TGA curves of CMS-SH, CMS-SS-NH_2, and CMS-SS-oHA are shown in Figure 4B. The ca. 6% weight loss of CMS-SS-oHA over a temperature range from 50 to 150 °C was due to adsorbed water. Compared with the weight loss of CMS-SS-NH_2, an additional weight loss of about 7% of CMS-SS-oHA was ascribed to the removal of oHA polymer on the surface of CMS. The TGA results further supported the ζ-potential data.

The 6-MP loading efficiency was measured on a UV−vis spectrophotometer before the release studies. The 6-MP loading efficiency of CMS-SS-MP/oHA and CMS-SH/6-MP was 4.1% and 2.8%, respectively. This result showed that 6-MP was more easily loaded into the mesopores of CMS by disulfide bonds than by simple physical adsorption.

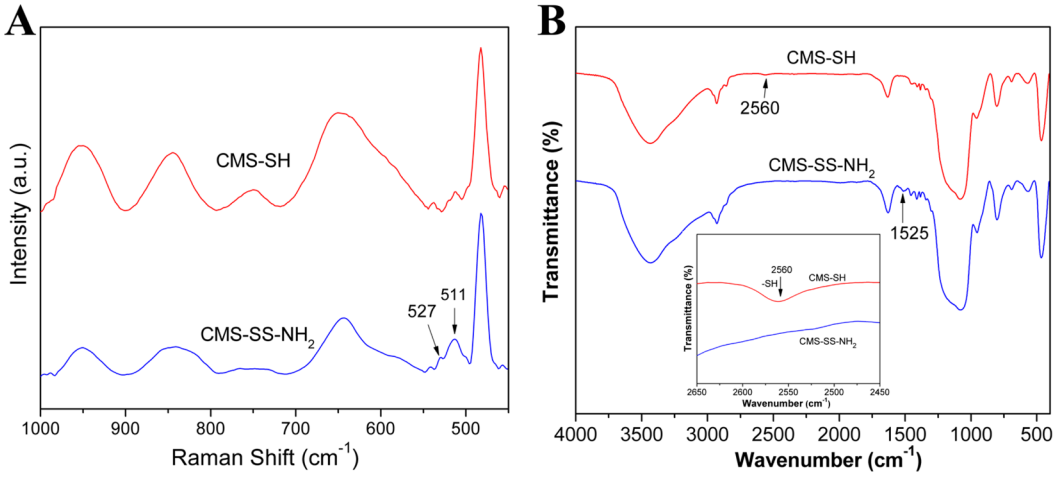

Figure 3. Raman spectra (A) and FT-IR spectra (B) of CMS-SH and CMS-SS-NH_2.

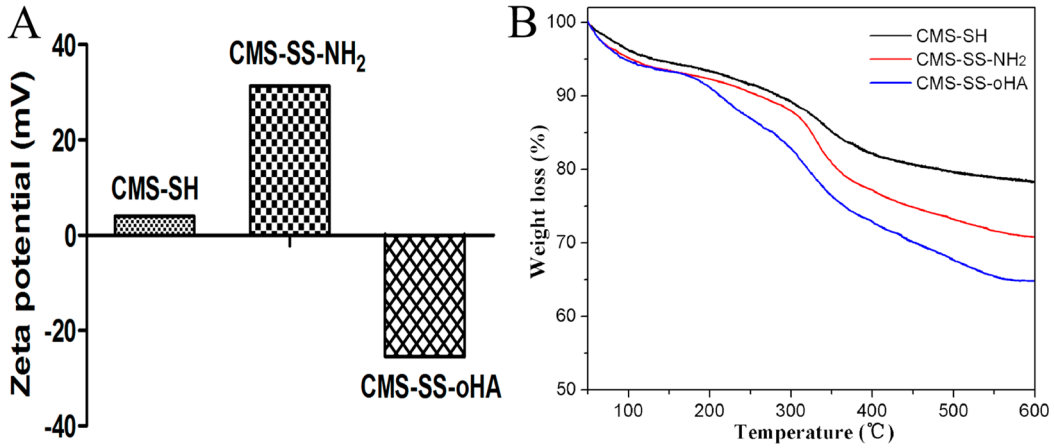

Figure 4. (A) Corresponding ζ-potentials of nanoparticles measured at each step of the drug loading process, and (B) TGA curves of CMS-SH, CMS-SS-NH_2, and CMS-SS-oHA.

3.3. Redox-Responsive Drug Release. The cumulative release curves of 6-MP from CMS-SS-MP/oHA and CMS/MP are shown in Figure 5. The CMS/MP sample (6-MP loaded into CMS-SH by physical adsorption) exhibited rapid release with a cumulative release rate of more than 85% within 1 h. In contrast, no premature release was observed from CMS-SS-MP/oHA in the absence of GSH within a period of 10 h, indicating "zero-release" of the redox-responsive DDS. However, in the presence of 3 mM GSH, CMS-SS-MP/oHA with drug conjugated to CMS by disulfide bonds exhibited redox-responsive release, and the cumulative release reached more than 80% within 2 h. When 1 mM GSH was present in the release fluids, CMS-SS-MP/oHA also exhibited redox-responsive release with the cumulative release percent of more than 30% within 2 h. Redox-responsive release is particularly important for targeted drug delivery.

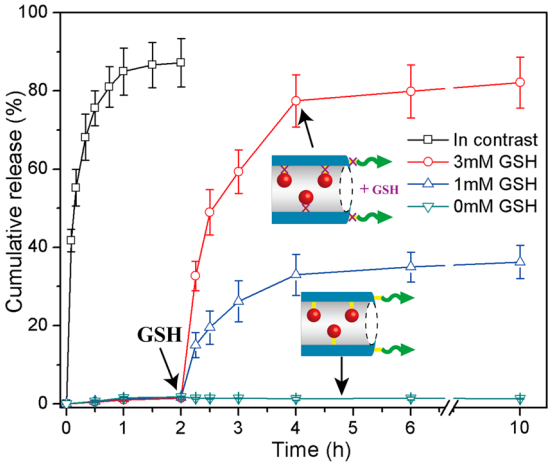

Figure 5. Cumulative release profiles of 6-MP from CMS-SS-MP/oHA in pH 7.4 PBS in the presence of different concentrations of GSH.

3.4. Dispersity and Stability of CMS-SS-oHA. Generally, MSNs cannot be used for intravenous injection directly, because the silica will agglomerate under physiological conditions or in saline solutions due to the destruction of the original interparticle charge−equilibrium in salt-containing solutions.[33] To overcome this problem, oHA was used to increase the dispersity and stability of CMS. The mean hydrodynamic diameter of CMS-SH and CMS-SS-oHA was measured in distilled water. The diameter of CMS-SH was 158 nm with a PDI of 0.267, greater than that observed from TEM owing to the hydrated diameter in aqueous medium. Although CMS-SS-oHA had a greater diameter (233 nm) than that of CMS-SH due to the grafting of hydrophilic oHA chains, the PDI of CMS-SS-oHA (0.049) was much smaller than that of CMS-SH. As shown in Figure 6A, although CMS-SH was stable in distilled water, CMS-SH nanoparticles flocculated rapidly after sonication in physiological PBS. However, the stability of CMS-SS-oHA was dramatically improved after conjugation with oHA chains in PBS and DMEM containing 10% FBS. As shown in Figure 6B,C, there was no obvious change in the hydrodynamic diameter of CMS-SS-oHA and the turbidity of CMS-SS-oHA solution in pH 7.4 PBS and water medium for 48 h. The markedly improved dispersity of CMS-SS-oHA compared with CMS-SH could be mainly attributed to the electrostatic repulsions between the hydrophilic oHA chains and the steric hindrance between the nanoparticles.

3.5. Hemolytic Behavior and BSA Adsorption of CMS-SH and CMS-SS-oHA. The hemolytic images of CMS-SH and CMS-SS-oHA over the concentration range from 20 to 1500 μg mL^{-1} are shown in Figure 7A. The CMS-SS-oHA nanoparticles showed excellent dispersibility and stability in PBS containing blood cells at high concentrations up to 1500 μg mL^{-1}. The percentage hemolysis of RBCs was calculated and shown in Figure 7B. The percentage hemolysis of CMS-SH is related to the concentration over a wide concentration range of 20 to 1500 μg mL^{-1}. When the concentration of CMS-SH reached 500, 1000, and 1500 μg mL^{-1}, the percentage hemolysis was 21.3%, 57.6%, and 66.5%, respectively. The high degree of hemolysis raised serious safety concerns regarding the application of MSNs for drug delivery. Some explanations for the hemolysis have been proposed, including reactive oxygen species (ROS) induced by the surface of the silica,[34,35] denaturation of membrane proteins via electrostatic interactions with silicate,[36] and the high affinity of silica for binding with tetra-alkyl ammonium groups that are plentiful in RBCs membranes.[35,37] So, modification of the biocompatible polymer chains on the surface of CMS can significantly reduce ROS, and the electrostatic interactions between silicate and membrane proteins, as well as the affinity between CMS and the tetra-alkyl ammonium groups. As expected, the percentage hemolysis of CMS-SS-oHA fell significantly to ca. 1% at an extremely high

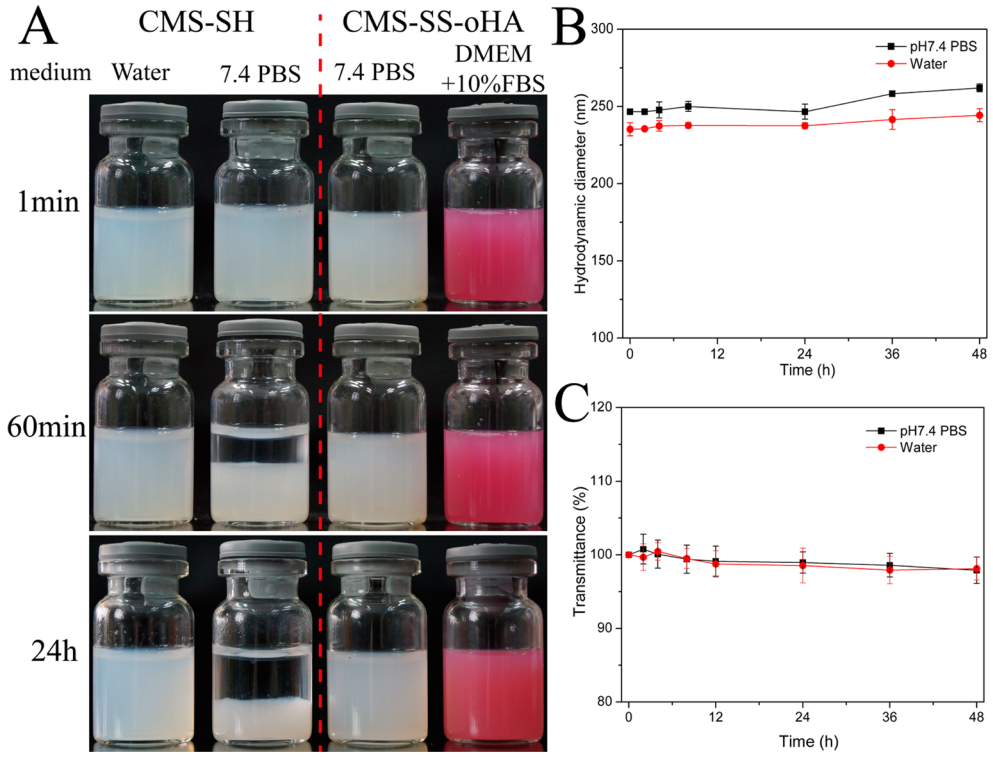

Figure 6. (A) Photographs of CMS and CMS-SS-oHA dispersed in different medium with a concentration of 5 mg/mL. All these photographs are taken at different times after dispersion by sonication. The stability of CMS-SS-oHA measured by dynamic light scattering (B) and turbidity (C) in pH 7.4 PBS and water.

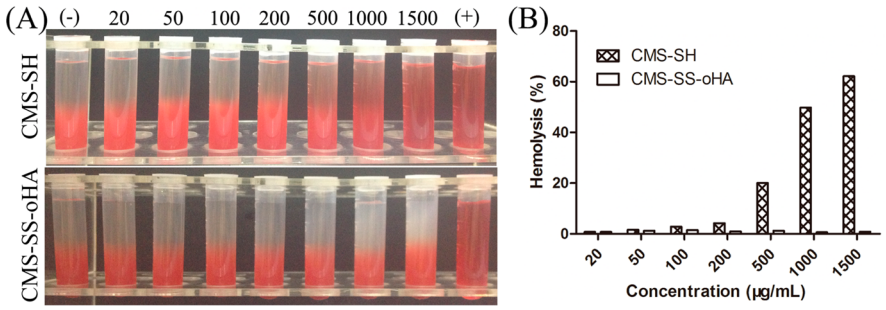

Figure 7. (A) Hemolytic photographs and (B) hemolysis percentages of CMS-SH and CMS-SS-oHA at different concentrations (μg mL^{-1}).

concentration (1500 μg mL^{-1}). Hence, oHA can improve the biocompatibility of CMS when administered intravenously.

The BSA adsorbed to the surface of CMS-SH and CMS-SS-oHA was measured to evaluate the effectiveness of the oHA modification. The oHA-modified CMS-SS-oHA markedly reduced the adsorbance of BSA from 2.06 wt % (CMS-SH) to 0.24 wt %. One possible explanation was that this was mainly attributable to the steric hindrance of oHA chains and the negative potential of CMS-SS-oHA. Hence, modification of oHA is a simple and effective method for increasing the biocompatibility, reducing the protein adsorption and improving the dispersity of silica, which would improve the active targeting efficiency and increase the permeation and retention (EPR) effect by prolonging the blood circulation time.

3.6. Cellular Uptake of CMS-SS-oHA and CMS-SH. HCT-116 and NIH-3T3 cells were used to evaluate the cellular uptake of FITC labeled CMS-SS-oHA and CMS nanoparticles. HCT-116 shows high expression levels of CD44 receptors, and NIH-3T3 is used as a negative cell line. To visualize the cellular uptake performance of the nanoparticles, both CMS-SS-oHA and CMS-SH were labeled with FITC and studied by confocal microscopy. As shown in Figure 8A, HCT-116 cells took up more green fluorescence originating from FITC labeled CMS-SS-oHA than NIH-3T3 cells, indicating that CMS-SS-oHA is more readily taken up by HCT-116 cancer cells. Furthermore, when HCT-116 cells were pretreated with 5 mg mL^{-1} free oHA to block CD44 receptors prior to incubation with FITC labeled CMS-SS-oHA, the intracellular green fluorescence was also weaker compared with when the oHA group was absent.

To obtain a quantitative comparison, the cellular uptake of FITC labeled CMS-SS-oHA and CMS nanoparticles in HCT-116 and NIH-3T3 cells is further studied by FACS analysis. Figure 8B shows that the mean fluorescence intensity (MFI) of CMS-SS-oHA increased 1.8-fold in HCT-116 cells compared with the MFI in NIH-3T3 cells. However, there were no obvious differences in the MFI of CMS-SH between HCT-116 and NIH-3T3 cells. The MFI of CMS-SS-oHA was weaker than that of CMS-SH in NIH-3T3 cells, because the fluorescence of FITC-labeled CMS-SS-oHA was reduced after the grafting of oHA. The reduced fluorescence might be due to the fact that

dx.doi.org/10.1021/am505824d | ACS Appl. Mater. Interfaces 2014, 6, 20290−20299

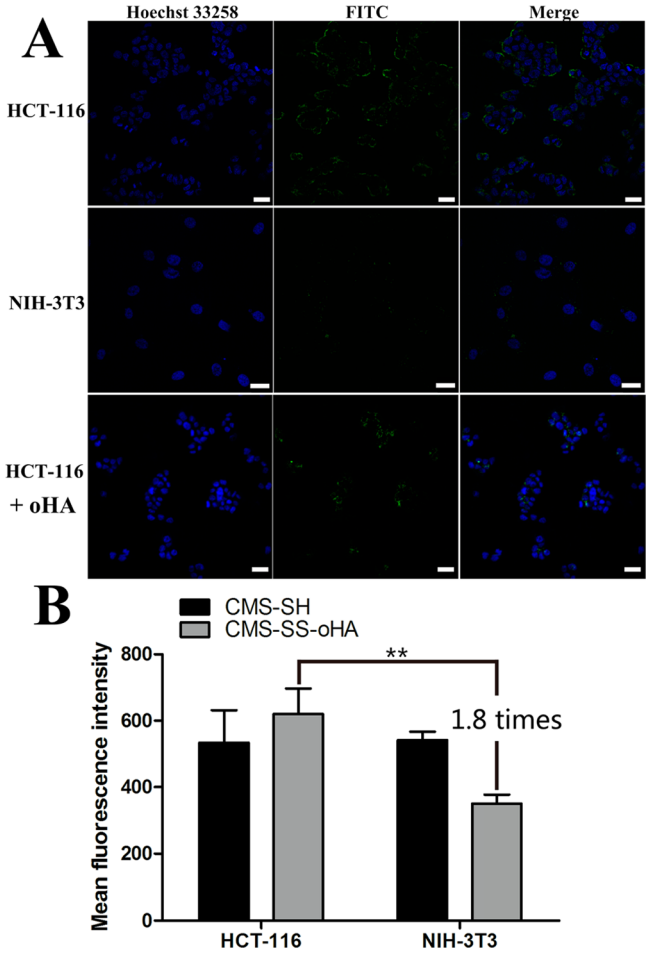

Figure 8. (A) CLSM images of specific endocytosis of FITC labeled CMS-SS-oHA nanoparticles by HCT-116, NIH-3T3 cells and HCT-116 cells pretreated with free oHA (5 mg mL^{-1}). Hoechst 33258 stained nucleus is seen in blue channel, and FITC labeled CMS-SS-oHA is seen in green channel. Bar represents 25 μm. (B) MFI of FITC labeled CMS-SS-oHA and CMS-SH in HCT-116 and NIH-3T3 cells was measured by FACS. Data are expressed as mean ± SD (n = 3). $^{**}p < 0.01$.

the weight was increased after the grafting of oHA, and some of the fluorescence was quenched after the modification process. To prove this hypothesis, the fluorescence intensity of FITC-labeled CMS-SH before and after oHA grafting were recorded on a microplate reader. It was found that the fluorescence intensity of FITC labeled CMS-SS-oHA reduced 55% compared with that of FITC labeled CMS-SH at a concentration of 100 μg mL^{-1}. Hence, the obtained results confirmed our assumption. These results demonstrate that the oHA modified on the surface of the CMS nanoparticles could specifically increase the binding affinity for CD44 receptors and, thus, increase the cellular uptake of CMS-SS-oHA in HCT-116 cells.

To further confirm that the target-specific uptake of FITC-labeled CMS-SS-oHA nanoparticles was mediated by CD44 receptors, an experiment involving free oHA or a low temperature was carried out. As shown in Figure 9, the MFI decreased to 70% of that of the untreated group when HCT-116 cells were incubated with 5 mg mL^{-1} oHA for 2 h before the addition of CMS-SS-oHA, which indicated that the free oHA reduced the uptake of CMS-SS-oHA via competitive

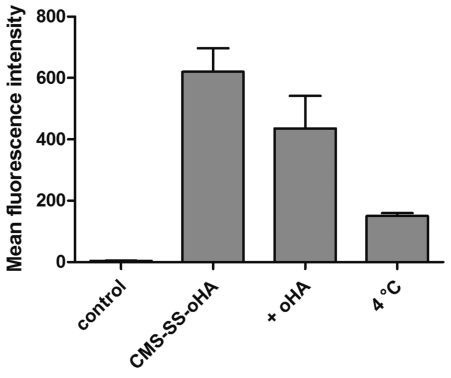

Figure 9. Intracellular MFI of FITC-labeled CMS-SS-oHA was analyzed by FACS. Alternatively, free oHA was added or cells were kept at 4 °C.

binding to CD44 receptors on the surface of HCT-116 cells. In addition, the uptake of CMS-SS-oHA appeared to be inhibited when experiments were performed at 4 °C, because receptor-mediated endocytosis involves ATP-dependent internalization and is relatively inactive at a low temperature. Hence, the clear suppression of cellular uptake by the addition of free oHA or 4 °C indicated that the internalization of CMS-SS-oHA nanoparticles was mostly mediated by CD44 receptors.

3.6. In Vitro Cytotoxicity Studies. HCT-116 and NIH-3T3 cells lines were selected for the cytotoxicity testing of CMS-SS-MP/oHA. As shown in Figure 10a,b, the cell viability of both cell lines incubated with blank CMS-SS-oHA nanoparticles was above 80% within the examined concentration range, demonstrating the good safety of the carriers.

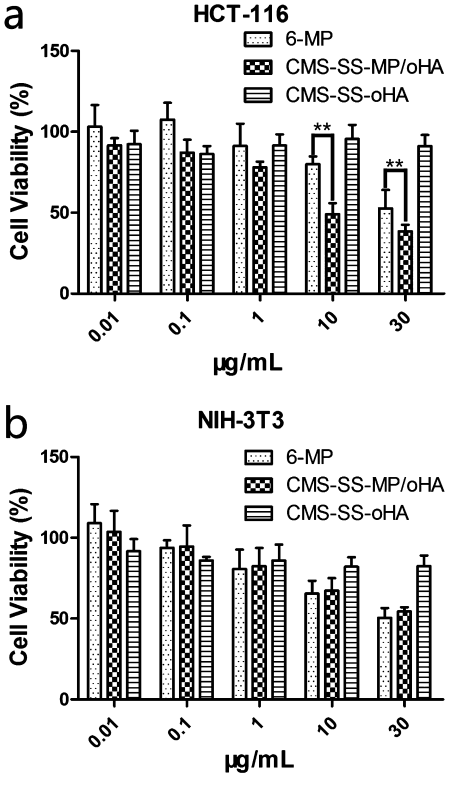

Figure 10. Cytotoxicity of free 6-MP, CMS-SS-MP/oHA, and CMS-SS-oHA against HCT-116 (a) and NIH-3T3 (b) cells at different concentrations. Data are expressed as mean ± SD (n = 3). $^{**}p < 0.01$.

dx.doi.org/10.1021/am505824d | ACS Appl. Mater. Interfaces 2014, 6, 20290−20299

HCT-116 and NIH-3T3 cells treated with free 6-MP and CMS-SS-MP/oHA show a 6-MP dose-dependent behavior. There was no significant difference in cell viability incubation with 6-MP between HCT-116 and NIH-3T3 cells lines. The viability of NIH-3T3 cells after incubation with CMS-SS-MP/oHA for 72 h at the concentrations of 10 and 30 μg mL^{-1} was 67.3% and 49.1%, respectively. In contrast, the viability of HCT-116 cells incubation with the same concentration of CMS-SS-MP/oHA reduced to 49.1% and 38.5%, respectively. The viability between the two cells were significantly different with the p values both less than 0.01 at the concentrations of 10 and 30 μg mL^{-1}. This increased cytotoxicity of CMS-SS-MP/oHA against HCT-116 could be explained by the improved cellular uptake of CMS-SS-oHA via oHA receptor-mediated endocytosis.[23,24]

4. CONCLUSIONS

In summary, a redox-responsive DDS based on CMS has been developed. The mercapto-containing drug 6-MP and the targeting ligand oHA were conjugated to the interior and exterior of CMS via cleavable disulfide bonds. The oHA was able to increase the stability and biocompatibility of CMS under physiological conditions. The in vitro release results indicated that CMS-SS-oHA exhibited highly redox-responsive release. The cellular uptake studies showed that FITC labeled CMS-SS-oHA exhibited a higher uptake performance against HCT-116 cells via CD44 receptor-mediated endocytosis compared with CMS. Furthermore, 6-MP loaded CMS-SS-oHA was more cytotoxic to HCT-116 cells than receptor-negative NIH-3T3 cells. All in all, the redox-responsive targeted DDS can deliver the mercapto-containing drug to specific target sites without any associated drug release, and be internalized via CD44 receptor-mediated endocytosis, and then the drug is released in the cytoplasm of the tumor cells.

AUTHOR INFORMATION

Corresponding Author

*S. Wang. Tel./fax: +86 24 23986348. E-mail: silingwang@syphu.edu.cn.

Notes

The authors declare no competing financial interest.

ACKNOWLEDGMENTS

This work was supported by National Basic Research Program of China (973 Program) (No. 2015CB932100) and National Natural Science Foundation of China (No. 81473165).

REFERENCES

(1) Langer, R. Drug Delivery and Targeting. *Nature* **1998**, *392*, 5−10.
(2) Soppimath, K. S.; Aminabhavi, T. M.; Kulkarni, A. R.; Rudzinski, W. E. Biodegradable Polymeric Nanoparticles as Drug Delivery Devices. *J. Controlled Release* **2001**, *70*, 1−20.
(3) Chen, W.; Zhong, P.; Meng, F.; Cheng, R.; Deng, C.; Feijen, J.; Zhong, Z. Redox and pH-Responsive Degradable Micelles for Dually Activated Intracellular Anticancer Drug Release. *J. Controlled Release* **2013**, *169*, 171−179.
(4) Guo, R.; Li, L. L.; Zhao, W. H.; Chen, Y. X.; Wang, X. Z.; Fang, C. J.; Feng, W.; Zhang, T. L.; Ma, X.; Lu, M.; Peng, S. Q.; Yan, C. H. The Intracellular Controlled Release from Bioresponsive Mesoporous Silica with Folate as Both Targeting and Capping Agent. *Nanoscale* **2012**, *4*, 3577−3583.
(5) Kim, T.-W.; Slowing, I. I.; Chung, P.-W.; Lin, V. S.-Y. Ordered Mesoporous Polymer−Silica Hybrid Nanoparticles as Vehicles for the Intracellular Controlled Release of Macromolecules. *ACS Nano* **2010**, *5*, 360−366.
(6) Lee, C. H.; Cheng, S. H.; Huang, I.; Souris, J. S.; Yang, C. S.; Mou, C. Y.; Lo, L. W. Intracellular pH-Responsive Mesoporous Silica Nanoparticles for the Controlled Release of Anticancer Chemotherapeutics. *Angew. Chem., Int. Ed.* **2010**, *122*, 8390−8395.
(7) Park, C.; Kim, H.; Kim, S.; Kim, C. Enzyme Responsive Nanocontainers with Cyclodextrin Gatekeepers and Synergistic Effects in Release of Guests. *J. Am. Chem. Soc.* **2009**, *131*, 16614−16615.
(8) Duan, X.; Xiao, J.; Yin, Q.; Zhang, Z.; Yu, H.; Mao, S.; Li, Y. Smart pH-Sensitive and Temporal-Controlled Polymeric Micelles for Effective Combination Therapy of Doxorubicin and Disulfiram. *ACS Nano* **2013**, *7*, 5858−5869.
(9) Cheng, R.; Feng, F.; Meng, F.; Deng, C.; Feijen, J.; Zhong, Z. Glutathione-Responsive Nano-vehicles as a Promising Platform for Targeted Intracellular Drug and Gene Delivery. *J. Controlled Release* **2011**, *152*, 2−12.
(10) Saito, G.; Swanson, J. A.; Lee, K.-D. Drug Delivery Strategy Utilizing Conjugation via Reversible Disulfide Linkages: Role and Site of Cellular Reducing Activities. *Adv. Drug Delivery Rev.* **2003**, *55*, 199−215.
(11) Torchilin, V. P. Recent Advances with Liposomes as Pharmaceutical Carriers. *Nat. Rev. Drug Discovery* **2005**, *4*, 145−160.
(12) Zhao, Y.; Vivero-Escoto, J. L.; Slowing, I. I.; Trewyn, B. G.; Lin, V. S. Capped Mesoporous Silica Nanoparticles as Stimuli-Responsive Controlled Release Systems for Intracellular Drug/Gene Delivery. *Exp. Opin. Drug Delivery* **2010**, *7*, 1013−1029.
(13) Chen, C.; Geng, J.; Pu, F.; Yang, X.; Ren, J.; Qu, X. Polyvalent Nucleic Acid/Mesoporous Silica Nanoparticle Conjugates: Dual Stimuli-Responsive Vehicles for Intracellular Drug Delivery. *Angew. Chem., Int. Ed.* **2011**, *50*, 882−886.
(14) Wang, X.; Cai, X.; Hu, J.; Shao, N.; Wang, F.; Zhang, Q.; Xiao, J.; Cheng, Y. Glutathione-Triggered "off-on" Release of Anticancer Drugs from Dendrimer-Encapsulated Gold Nanoparticles. *J. Am. Chem. Soc.* **2013**, *135*, 9805−9810.
(15) Ahn, B.; Park, J.; Singha, K.; Park, H.; Kim, W. J. Mesoporous Silica Nanoparticle-based Cisplatin Prodrug Delivery and Anticancer Effect Under Reductive Cellular Environment. *J. Mater. Chem. B* **2013**, *1*, 2829−2836.
(16) Stern, R.; Jedrzejas, M. J. Hyaluronidases: Their Genomics, Structures, and Mechanisms of Action. *Chem. Rev.* **2006**, *106*, 818−839.
(17) Toole, B. P. Hyaluronan: From Extracellular Glue to Pericellular Cue. *Nat. Rev. Cancer* **2004**, *4*, 528−539.
(18) Surace, C.; Arpicco, S.; Dufaÿ-Wojcicki, A. l.; Marsaud, V. r.; Bouclier, C. l.; Clay, D.; Cattel, L.; Renoir, J.-M.; Fattal, E. Lipoplexes Targeting the CD44 Hyaluronic Acid Receptor for Efficient Transfection of Breast Cancer Cells. *Mol. Pharmaceutics* **2009**, *6*, 1062−1073.
(19) Choi, K. Y.; Yoon, H. Y.; Kim, J.-H.; Bae, S. M.; Park, R.-W.; Kang, Y. M.; Kim, I.-S.; Kwon, I. C.; Choi, K.; Jeong, S. Y. Smart Nanocarrier Based on PEGylated Hyaluronic Acid for Cancer Therapy. *ACS Nano* **2011**, *5*, 8591−8599.
(20) Ma, M.; Chen, H.; Chen, Y.; Zhang, K.; Wang, X.; Cui, X.; Shi, J. Hyaluronic Acid-conjugated Mesoporous Silica Nanoparticles: Excellent Colloidal Dispersity in Physiological Fluids and Targeting Efficacy. *J. Mater. Chem.* **2012**, *22*, 5615.
(21) Yu, M.; Jambhrunkar, S.; Thorn, P.; Chen, J.; Gu, W.; Yu, C. Hyaluronic Acid Modified Mesoporous Silica Nanoparticles for Targeted Drug Delivery to CD44-Overexpressing Cancer Cells. *Nanoscale* **2013**, *5*, 178−183.
(22) Chen, Z.; Li, Z.; Lin, Y.; Yin, M.; Ren, J.; Qu, X. Bioresponsive Hyaluronic Acid-Capped Mesoporous Silica Nanoparticles for Targeted Drug Delivery. *Chem.—Eur. J.* **2013**, *19*, 1778−1783.
(23) Yang, C.; Cao, M.; Liu, H.; He, Y.; Xu, J.; Du, Y.; Liu, Y.; Wang, W.; Cui, L.; Hu, J.; Gao, F. The High and Low Molecular Weight Forms of Hyaluronan Have Distinct Effects on CD44 Clustering. *J. Biol. Chem.* **2012**, *287*, 43094−43107.
(24) Yang, C.; Liu, Y.; He, Y.; Du, Y.; Wang, W.; Shi, X.; Gao, F. The Use of HA Oligosaccharide-Loaded Nanoparticles to Breach the

Endogenous Hyaluronan Glycocalyx for Breast Cancer Therapy. *Biomaterials* **2013**, *34*, 6829−6838.
(25) Platt, V. M.; Szoka, F. C., Jr. Anticancer Therapeutics: Targeting Macromolecules and Nanocarriers to Hyaluronan or CD44, a Hyaluronan Receptor. *Mol. Pharmaceutics* **2008**, *5*, 474−486.
(26) Cui, Y.; Dong, H.; Cai, X.; Wang, D.; Li, Y. Mesoporous Silica Nanoparticles Capped with Disulfide-Linked PEG Gatekeepers for Glutathione-Mediated Controlled Release. *ACS Appl. Mater. Interfaces* **2012**, *4*, 3177−3183.
(27) Möller, K.; Kobler, J.; Bein, T. Colloidal Suspensions of Mercapto-Functionalized Nanosized Mesoporous Silica. *J. Mater. Chem.* **2007**, *17*, 624−631.
(28) Ebright, Y. W.; Chen, Y.; Kim, Y.; Ebright, R. H. S-[2-(4-Azidosalicylamido)ethylthio]-2-thiopyridine: Radioiodinatable, Cleavable, Photoactivatible Cross-Linking Agent. *Bioconjugate Chem.* **1996**, *7*, 380−384.
(29) He, Q.; Zhang, J.; Shi, J.; Zhu, Z.; Zhang, L.; Bu, W.; Guo, L.; Chen, Y. The Effect of PEGylation of Mesoporous Silica Nanoparticles on Nonspecific Binding of Serum Proteins and Cellular Responses. *Biomaterials* **2010**, *31*, 1085−1092.
(30) Gu, J.; Su, S.; Zhu, M.; Li, Y.; Zhao, W.; Duan, Y.; Shi, J. Targeted Doxorubicin Delivery to Liver Cancer Cells by PEGylated Mesoporous Silica Nanoparticles with a pH-Dependent Release Profile. *Micropor. Mesopor. Mater.* **2012**, *161*, 160−167.
(31) Okabayashi, H.; Izawa, K.; Yamamoto, T.; Masuda, H.; Nishio, E.; O'Connor, C. Surface Structure of Silica Gel Reacted with 3-Mercaptopropyltriethoxysilane and 3-Aminopropyltriethoxysilane: Formation of the S−S Bridge Structure and Its Characterization by Raman Scattering and Diffuse Reflectance Fourier Transform Spectroscopic Studies. *Colloid Polym. Sci.* **2002**, *280*, 135−145.
(32) Hunter, R. J. *Zeta Potential in Colloid Science: Principles and Applications*; Academic Press: London, 1981; Vol. *125*.
(33) Wang, L.-S.; Wu, L.-C.; Lu, S.-Y.; Chang, L.-L.; Teng, I.-T.; Yang, C.-M.; Ho, J.-a. A. Biofunctionalized Phospholipid-Capped Mesoporous Silica Nanoshuttles for Targeted Drug Delivery: Improved Water Suspensibility and Decreased Nonspecific Protein Binding. *ACS Nano* **2010**, *4*, 4371−4379.
(34) Nash, T.; Allison, A.; Harington, J. Physico-chemical Properties of Silica in Relation to Its Toxicity. *Nature* **1966**, *210*, 259−261.
(35) Slowing, I. I.; Wu, C. W.; Vivero-Escoto, J. L.; Lin, V. S. Y. Mesoporous Silica Nanoparticles for Reducing Hemolytic Activity Towards Mammalian Red Blood Cells. *Small* **2009**, *5*, 57−62.
(36) Diociaiuti, M.; Bordi, F.; Gataleta, L.; Baldo, G.; Crateri, P.; Paoletti, L. Morphological and Functional Alterations of Human Erythrocytes Induced by SiO_2 Particles: An Electron Microscopy and Dielectric Spectroscopy Study. *Environ. Res.* **1999**, *80*, 197−207.
(37) Depasse, J.; Warlus, J. Relation Between the Toxicity of Silica and Its Affinity for Tetraalkylammonium Groups. Comparison Between SiO_2 and TiO_2. *J. Colloid Interface Sci.* **1976**, *56*, 618−621.